MODELING SEASONAL STRATOSPHERIC SUDDEN WARMING CLIMATOLOGY BASED ON POLAR VORTEX STATISTICS

by

Matthew Francis Horan

A thesis submitted to the faculty of
The University of Utah
in partial fulfillment of the requirements for the degree of

Master of Science

Department of Atmospheric Sciences

The University of Utah

August 2017

The University of Utah Graduate School

STATEMENT OF THESIS APPROVAL

The thesis of **Matthew Francis Horan**

has been approved by the following supervisory committee members:

Thomas Reichler	, Chair	**03/22/17** Date Approved
William James Steenburgh	, Member	**03/22/17** Date Approved
Courtenay Strong	, Member	**03/22/17** Date Approved

and by **Kevin Perry** , Chair/Dean of

the Department/College/School of **Atmospheric Sciences**

and by David B. Kieda, Dean of The Graduate School.

ABSTRACT

The downward influence of stratospheric sudden warmings (SSWs) can create significant tropospheric circulation anomalies that last for several weeks. It is therefore of interest to understand the month of the year during which SSWs are most likely to occur and the controlling factors of their temporal distribution. Conceivably, the distribution is controlled by the interplay between decreasing stratospheric wave driving and weakening stratospheric vortex strength. General circulation models (GCMs) tend to produce their SSW maximum later in winter than observations, which is considered a model deficiency. However, the observed record is short, suggesting that under-sampling of SSWs may contribute to this discrepancy. Here, we study the distribution of SSWs and related events in a long control simulation with a stratosphere resolving GCM. Further, we create a simple statistical model to determine the primary factors controlling the SSW distribution. The model is based on the daily climatological mean, standard deviation, and autocorrelation of stratospheric winds and assumes that the winds follow a normal distribution. Results indicate that we cannot reject the null hypothesis that model and observations stem from the same distribution suggesting that the mid-winter SSW maximum seen in the observations is due to sampling uncertainty. We conclude that the late SSW distribution seen in models is not unrealistic and that it is likely that future observations will show more late winter SSWs. We further find that the statistical model reproduces the seasonal evolution of SSWs well and that the decreasing climatological

strength of the vortex is the primary factor in controlling the SSW distribution. This supports the idea that stratospheric winds are approximately normally distributed and that SSWs simply form the tail of this monotonic and unimodal distribution.

TABLE OF CONTENTS

LIST OF FIGURES

Figures

ACKNOWLEDGEMENTS

I would like to gratefully acknowledge the Air Force Institute of Technology program for the financial and logistical support. Partial funding for this research was provided by the National Science Foundation under grant 1446292. I would also like to acknowledge the Center for High Performance Computing for providing technological assistance through the program.

I would like to thank Thomas Reichler, my advisor, for the guidance and direction for the past 19 months. I would also like to acknowledge the outstanding faculty of the Department of Atmospheric Sciences and the remainder of my supervisory committee for their teachings and final suggestions for this work.

Finally, I would like to thank my family and friends as a whole, from near and far, for the moral support and patience through the process. Without you, this may have never been completed.

CHAPTER 1

INTRODUCTION

Accurate seasonal forecasts rely on knowledge of the state of the stratosphere (Sigmond et al. 2013). Long-term global fluctuations manifested in the stratosphere can be used to predict future states of the troposphere which could last for weeks (Baldwin and Dunkerton 2001; Ineson and Scaife 2009). One of the most prominent events which occur in the stratosphere is the stratospheric sudden warmings (SSW). The downward propagation after an SSW causes a negative phase of the Northern Annular Mode for up to two months after an event (Baldwin and Dunkerton 2001). This phase is associated with a southward shift in storm tracks and an increase in precipitation in Europe and the Eastern United States (Thompson et al. 2002; Kidston et al. 2015). Because SSWs are persistent, knowledge of when they are most likely to occur better prepares forecasters for the anomalies they cause.

Although some debate exists on how to define an SSW (Butler et al. 2015), Charlton and Polvani (2007, hereafter CP07) provide a widely used definition of major SSWs similar to what we use throughout this work. They base their definition on the zonal mean zonal wind at 10 hPa and 60°N (hereafter U1060). We consider only major SSWs, which require a reversal of direction of the polar vortex (represented by U1060), while ignoring minor warmings. Jucker (2016) argues that in longer idealized

simulations, with a large sample size of SSWs, any valid definition of SSWs produces results that have similar tropospheric impacts, although different definitions may show similar events occurring at separate times.

Previous studies (Charlton et al. 2007; Charlton-Perez et al. 2008; Butchart et al. 2011) note that reanalysis tends to favor SSWs occurring in mid-winter, while many general circulation models (GCMs) tend to favor SSWs during late winter. These studies use the monthly distribution of SSWs as an indicator of how well GCMs portray the seasonal distribution of SSWs. However, as SSWs are rare events, occurring slightly more than once every two years (Butler et al. 2015), the observed SSW sample size for each individual month is small. In the NCEP/NCAR Reanalysis (NNR, Kalnay et al. 1996), there are fewer than ten SSWs in each month, creating large uncertainty in the shape of the seasonal distribution. Accordingly, the first goal of this study is to decide whether the difference between the seasonal distribution of SSWs in models and observations are statistically significant and determine what factors lead to the seasonal maximum in SSWs.

SSWs are caused by the convergence of vertically propagating planetary waves creating easterly accelerations in the stratospheric winds (Matsuno, 1971). Evidence of the influence of planetary wave propagation is furthered by the fact that only one SSW has been observed in the Southern hemisphere (Charlton et al. 2005; Krüger et al. 2005), where less topographic forcing leads to fewer planetary waves in winter. Several SSWs have occurred in the Northern Hemisphere (CP07), where more topographic forcing leads to stronger stratospheric wave forcing (Kidston et al. 2015). Previous studies attribute the onset of SSWs to an increasing frequency of planetary waves propagating upward from

the troposphere to the stratosphere (Polvani and Waugh 2004; Limpasuvan et al. 2005). At the same time, a stronger polar vortex should require more wave forcing to reverse than a weaker polar vortex. It is therefore conceivable that later in winter, it takes weaker planetary wave propagation (and in turn less convergence) to influence the polar vortex enough to create an SSW. This planetary wave propagation, represented physically by the Eliassen-Palm (EP) flux (Holton and Hakim 2013), maximizes in mid-winter, near the same time as the maximum strength in U1060 (Fig. 1.1). Jucker (2016) argues that this increased propagation is not the primary trigger of an SSW, and that throughout Northern Hemisphere winter, there is enough upward wave propagation for an SSW to occur. Others argue that planetary wave propagation is only responsible for conditioning the polar vortex to favor SSWs, but the convergence of planetary waves is not responsible for the SSW itself (Albers and Birner 2014). Hence, as one goes from mid-winter to late winter and early spring, there is an interplay between the weakening strength of the polar vortex (leading to more SSWs) and the reduced amount of planetary wave driving (leading to fewer SSWs) occurring in late winter. If planetary wave propagation is the primary factor in the occurrence of SSWs, this should lead to a greater occurrence rate of SSWs in mid-winter, concurrent with the maximum in EP flux (Fig. 1.1). However, if polar vortex strength is the primary factor in SSW occurrence, we will observe most SSWs occurring in late winter, when the polar vortex is naturally weakening. Accordingly, the second goal of this research is to investigate the importance of the weakening polar vortex strength in controlling the frequency of SSWs. This is accomplished by statistically modelling the daily evolution of the probability of SSWs without directly considering the seasonal evolution of the planetary wave propagation.

More specifically, results are based on only the mean, standard deviation, and lagged autocorrelation of this distribution. We assume that the evolution of stratospheric winds follows multivariate normal distribution (Wilks 2006) and systematically analyze the influence of the individual requirements (CP07) on the occurrence of SSWs to determine where the sensitivity of the model lies, and the causes of any errors.

This work is structured as follows. Chapter 2 describes the data, methods, and assumptions we use in this work. Chapter 3 discusses the statistical model and the results thereof in terms of the input parameters and the observed occurrences in each dataset (hereafter empirical data). It then analyzes how our results compare to other models, and how sensitive our statistical model is to changes in the input parameters. Finally, Chapter 4 presents a summary of our findings, the conclusions we reach, and the potential for future work.

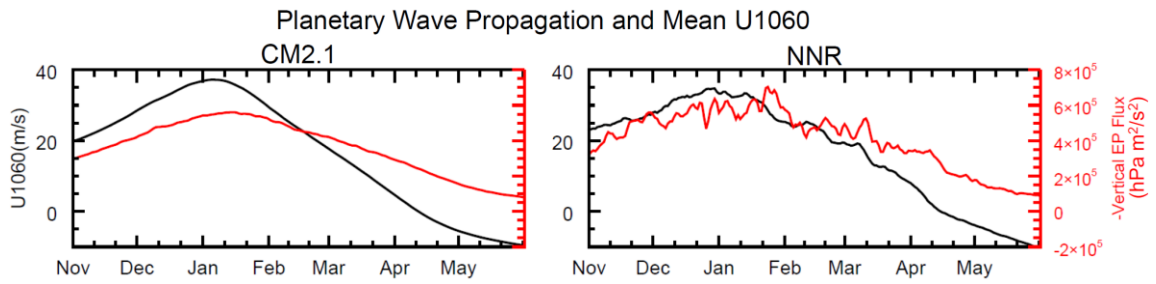

Fig. 1.1. Climatology of the seasonal cycle of U1060 and EP flux. Shown are (black) the climatology of the zonal mean zonal wind at 10 hPa and 60°N and (red) the zonal mean vertical Eliassen-Palm (EP) flux averaged from 45°N to 75°N at 100 hPa. EP flux has been multiplied by -1 so that the largest value represents the greatest upward propagation of planetary waves.

CHAPTER 2

METHODOLOGY

Most of our analysis is based on daily output from a nearly 10,000-year-long control run conducted with a stratosphere-resolving version of the Geophysical Fluid Dynamics Laboratory's (GFDL) climate model CM2.1 (Staten and Reichler 2013). The original version of the model (Delworth et al. 2006) has 24 vertical levels, while our version uses 48 vertical levels, with the additional levels being mostly concentrated in the stratosphere. Greenhouse gases and other external forcings are prescribed to the model at 1990 levels and held constant through time. The well-resolved stratosphere is necessary to portray a more accurate stratospheric circulation and frequency of SSWs (Charlton-Perez et al. 2013). We also use daily data from the 1948-2015 NNR and from select models used in the Fifth Coupled Model Intercomparison Project (CMIP5). For each of these datasets, we extract a long time series of U1060 to create two distributions: an empirical distribution based solely on the actual number of events which occur in the dataset itself and a statistical distribution, based on the model described below.

The daily climatologies of the mean, standard deviation, and skewness of U1060 are empirically derived from the investigated dataset and denoted $\mu(t)$, $\sigma(t)$, and $\gamma(t)$ respectively, where *t* denotes the day of the year. All values are smoothed in time using a Gaussian smoother with a kernel of three standard deviations. Additionally, we assign

$r(t,\tau)$ to the climatological lagged autocorrelation of U1060 for each day *t* and lag τ. One of the basic assumptions of this work is that on any given day, U1060 is approximately normally distributed. In other words, we assume that the most likely value of U1060 is at its daily mean and the actual values are evenly distributed around that mean following a Gaussian distribution. As we will show, this assumption is reasonable for most of our work.

In this work, we find the empirical frequency and statistical probability of the following four events:

1. *Zero Crossings* are defined as the days when U1060 shifts from westerly to easterly. Zero crossings can occur on any day of the year, but empirically do so only during fall, winter, and spring.
2. *Vortex Returns* are a special case of zero crossings which are additionally conditioned on 10 subsequent and consecutive days of positive values of U1060. The date of vortex returns occurs on the day of the first zero crossing, and by definition must occur between 1 November and 31 March.
3. *SSWs* are isolated vortex returns that are separated from each other by at least 20 days. Should two vortex returns occur within 20 days of each other, only the first is considered as an SSW.
4. *Final Warmings* are the final zero crossings of winter.

Our definition of SSWs, illustrated in Fig 2.1, differs slightly from that of CP07. We allow for 10 days of positive U1060 to occur on any day before 31 May (rather than 30 April as in CP07) to ensure all instances before the final warming are included. Additionally, in order to use the same data to find all four events, our definition of final

warmings differs from that of Black et al. (2006) who define final warmings based on the zonal mean zonal wind at 70°N and 50 hPa and the condition that the wind does not exceed five m/s after a zero crossing.

Zero crossings are rare events, and they form a requirement for all other events described above. In mid-winter, the relative frequency of easterlies in U1060 is very small (Fig. 2.2), and due to the highly persistent nature of stratospheric winds, the probability of a directional shift in the zonal winds is even smaller. Our statistical model aims to accurately portray the frequency of these low probability events while considering the low frequency of events and high persistence of U1060.

To find the probability of zero crossings on any given day *n*, we integrate a multivariate normal distribution in two dimensions using

$$P(ZC)_n = \int_{z_2'=-\infty}^{z_2'=-\frac{\mu_n}{\sigma_n}} \int_{z_1'=-\frac{\mu_{n-1}}{\sigma_{n-1}}}^{z_1'=\infty} \frac{1}{(2\pi)^{\frac{k}{2}}\sqrt{\det[\boldsymbol{R}]}} \exp\left[\frac{-\boldsymbol{z}^{\boldsymbol{T}}[\boldsymbol{R}]^{-1}\boldsymbol{z}}{2}\right] dz_1 dz_2 = P(U_n^- \cup U_{n-1}^+) \qquad (1)$$

(adapted from Wilks 2006), where $\boldsymbol{R}$ is a 2x2 lagged (for days *n*-1 and day *n*) correlation matrix, $\boldsymbol{z}$ is a vector $\begin{pmatrix} z_1 \\ z_2 \end{pmatrix}$ of normalized U1060 values for days *n-1* (z_1) and *n* (z_2) , and *k=2* is the dimensionality of the problem (i.e. the number of days considered). The ∪ symbol represents a union of multiple events The value $-\frac{\mu}{\sigma}$ in terms of normalized $\boldsymbol{z}$ constitutes the value of zero in the actual U distribution. Thus, the inner integral represents the probability that U1060 is positive on day *n-1*, denoted by $P(U_{n-1}^+)$. The outer integral represents the probability of U1060 being negative on day *n*, denoted by $P(U_n^-)$. We use an efficient numerical algorithm (Genz et al. 2004) to calculate multivariate integrals (like Eq. 1), but this algorithm does not allow us to incorporate the skewness of the distribution, so only the mean, standard deviation, and autocorrelations

are used as input parameters to our statistical model. If we could take skewness into account, it would lead to a more accurate representation of the negative tail of U1060 (Fig. 2.2). However, as we will show below, skewness is small during late winter when most SSWs occur, and therefore, the neglect of the skewness does not impact our results in major ways.

To find the probability of a vortex return on day *n* ($P(VR)_n$), we first use a similar calculation (described in detail in the Appendix) to find the probability of 10 consecutive days of westerly values of U1060 using a multivariate normal distribution. This can be represented as

$$P(VR^*)_n = [P(ZC)_n \cup U^+_{n+1} \cup U^+_{n+2} \ldots \cup U^+_{n+10}] + [P(ZC)_n \cup U^-_{n+1} \cup U^+_{n+2} \ldots \cup U^+_{n+11}] \ldots + [P(ZC)_n \cup U^-_{21\,May} \cup U^+_{22May} \ldots \cup U^+_{31\,May}]$$

where U^+_n represents the probability of a positive value of U1060 on day *n*.

Mathematically, this union is resolved by nested integrals similar to Eq. 1, and thus the above equation represents the sum of several equations which require either twelve or thirteen nested integrals (see Appendix). However, $P(VR^*)_n$ also includes the probability of multiple periods after the first zero crossing meeting the criteria. In order to account for this possibility, for all days after *n+12*, we remove the probability that vortex return criteria had already been fulfilled. For example, on day *n+31*, this probability can be described as

$$P(VR^{\#})_{n+31} = [P(ZC)_n \cup U^+_{n+1} \cup U^+_{n+2} \ldots \cup U^+_{n+10} \cup U^-_{n+30} \cup U^+_{n+31} \ldots \cup U^+_{n+40}] + [P(ZC)_n \cup U^-_{n+1} \cup U^+_{n+2} \ldots \cup U^+_{n+11} \cup U^-_{n+30} \cup U^+_{n+31} \ldots \cup U^+_{n+40}] \ldots + [P(ZC)_n \cup U^-_{n+19} \cup U^+_{n+20} \ldots \cup U^+_{n+29} \cup U^-_{n+30} \cup U^+_{n+31} \ldots \cup U^+_{n+40}]$$

where $P(VR^{\#})_n$ represents the probability that vortex return conditions are met on day *n*

but had already occurred on a prior day. The probability of vortex return conditions being met three or more times after a zero crossing in a winter is three orders of magnitude smaller than the probability of it to occur twice and is therefore ignored. To determine our overall probability of a vortex return, $P(VR)_n$, we calculate:

$$P(VR)_n = P(VR^*)_n - P(VR^\#)_{n+12} - P(VR^\#)_{n+13} \ldots - P(VR^\#)_{22\,May}$$

We cease calculating $P(VR^\#)$ after 22 May as 10 days of positive U1060 starting on that date would end on 31 May.

Once the chance of a vortex return is established, we determine as a final step if there are at least 20 days of separation between events (CP07). For this we treat each SSW as an independent event, which is a slight oversimplification as it does not take into account the persistent nature of SSWs, and therefore may create a very small overestimate of SSWs. We multiply the chance of a vortex return by the sum of chances of an SSW in the previous 20 days following

$$P(SSW)_n = P(VR)_n[1 - \textstyle\sum_{i=n-20}^{i=n-1} P(SSW)_i].$$

The result is the probability of an SSW with a central date of day *n*, assuming a multivariate normal distribution.

We use a similar methodology to determine the probability of final warmings, $P(FW)$. In order to determine the probability of a final warming on day *n*, we integrate Eq. 1 assuming day *n-1* has a positive value of U1060, while day *n* and all subsequent days through 31 May have negative values. This can be written as

$$P(FW) = P\left(U_{n-1}^{+} \cup U_n^{-} \cup U_{n+1}^{-} \ldots \cup U_{31\,May}^{-}\right).$$

As the positive requirement for day *n-1* creates mutually exclusive events, there is no need to adjust these results for multiple events.

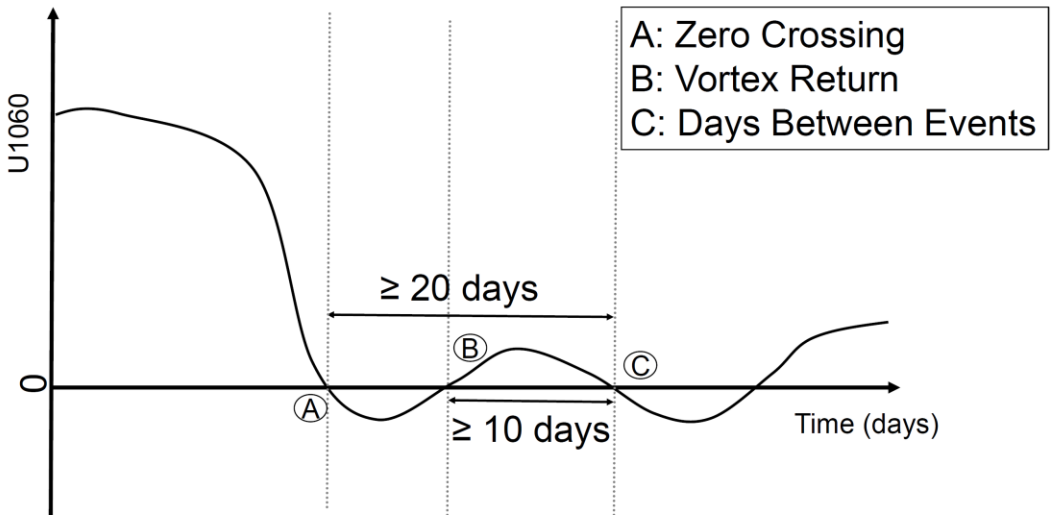

Fig. 2.1. SSW schematic. Shown is the idealized evolution of U1060 for a typical SSW. (A) indicates a zero crossing and (B) a vortex return. (C) represents the requirement that multiple SSWs in one season must be at least 20 days apart from each other.

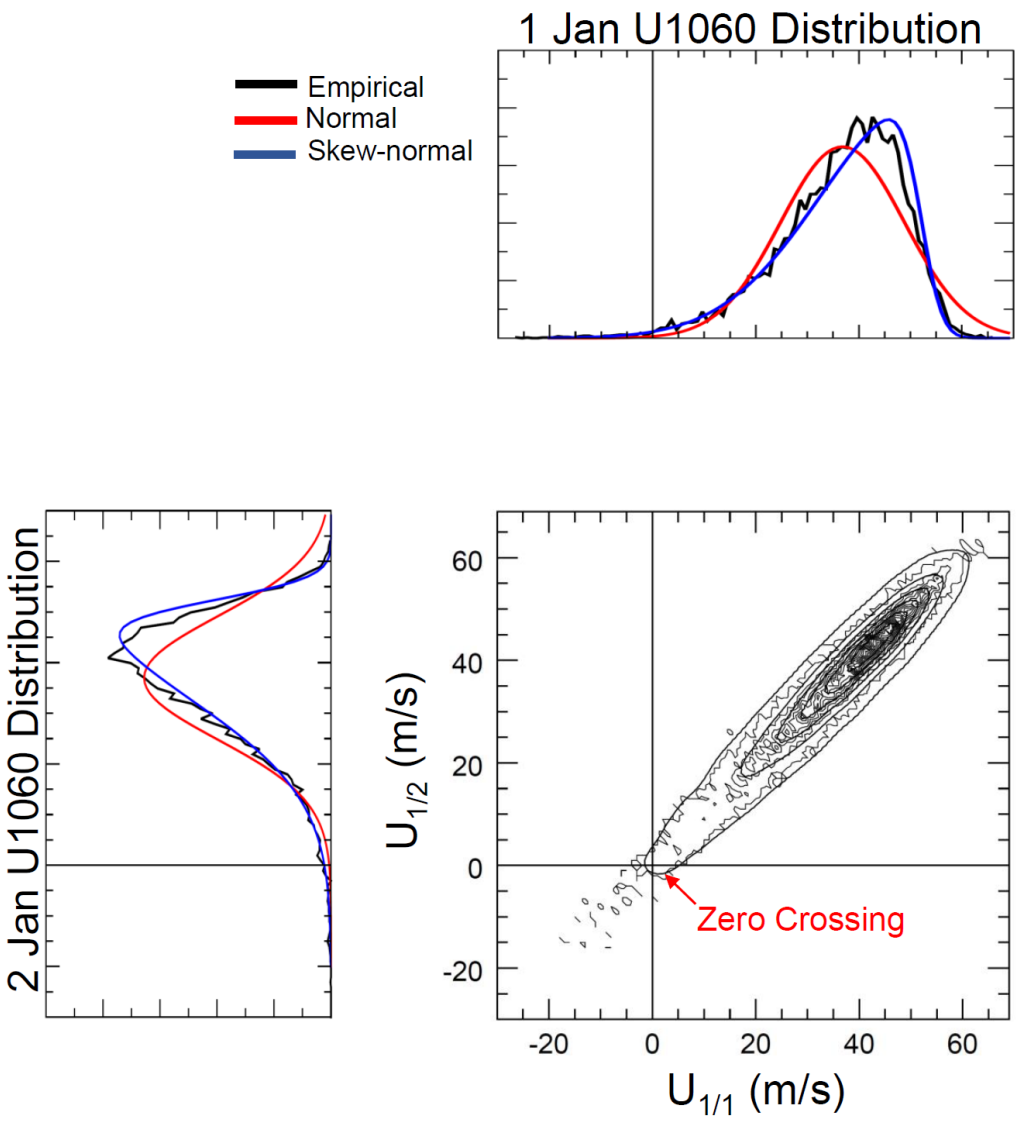

Fig. 2.2. Distribution of U1060 on 1 January and 2 January in CM2.1. (Top) shows the 1 January (black) empirical distribution, along with (red) normal and (blue) skew-normal (Azzalini 1985) distributions using parameters calculated from the empirical data. (Left) for 2 January. (Bottom right) shows the corresponding two-dimensional distribution. The first contour represents one event during the 10,000 samples, with a contour interval of five events. Bin size in all panels is 1 m/s. The arrow in the bottom right quadrant highlights zero crossings.

CHAPTER 3

RESULTS

Through the following, we attempt to statistically model the daily evolution of probability of an SSW using only the distribution of U1060 and an assumption of a multivariate normal distribution. This section builds on each criteria of an SSW to determine how well our statistical model determines the probability of each criteria (Fig. 2.1) in comparison to the empirical data.

3.1. SSW Seasonality

In evaluating our model simulated SSW seasonality with observed events from NNR, we note that the observed period from 1948 to 2015 is short. The resulting small sample size of SSWs (ten or fewer per month from the 67 winters) introduces large uncertainty to the seasonal distribution. We begin by comparing the seasonal distribution of SSWs in the model with the entire 67-winter NNR dataset and a shorter 45-winter timeframe analyzed by Charlton-Perez et al. (2008). When comparing 45 (Fig. 3.1a) or 67 (Fig. 3.1b) winters from CM2.1 to NNR by bootstrapping 10,000 times without replacement, the number of SSWs in NNR is within the 95% confidence interval of the model-derived SSW distributions . The overall number of SSWs in the observations is only slightly above the mean of the distributions taken from the model. When individual

months are considered, however, the number of SSWs in NNR is further from the mean. In NNR, December and January have more observed SSWs, while February and March have fewer than the model. January is in particular noteworthy since the observed number of SSWs is at the upper threshold of the 95% confidence interval. We cannot reject the null hypothesis that both distributions are from the same long-term dataset, but the difference in January cannot be fully ignored either. Also, using the 67-winter period of NNR shifts the month with the maximum number of SSWs from January to February, but uncertainty in the monthly distribution still remains high.

In order to further investigate the seasonality of SSWs, we reduce our bin size from the monthly timeframe to a running 11-day average (Fig. 3.1c). The maximum number of SSWs in both datasets is now at the end of February, suggesting that the January maximum seen in NNR (Fig. 3.1a) is sensitive to the arbitrary definition of months created by the Gregorian calendar. The difference between the two datasets stems from both the model showing fewer SSWs through December and January, and the observations having a relative minimum of SSWs in early February.

The late February maximum in both observations and the climate model is long after our maximum in both planetary wave propagation and polar vortex strength (Fig. 1.1) It is still early enough that it is probable that the polar vortex will reestablish (and thus become an SSW) after a zero crossing. This timing suggests that the decreasing polar vortex strength in late winter is a more important factor in the occurrence rate of SSWs than the varying amount of stratospheric wave driving. This represents the motivation for our attempt to determine the daily climatological probability of SSWs using only the statistical properties of U1060.

3.2. Input Parameters

The seasonal evolution of the moments and correlations of U1060 derived from NNR and CM2.1 are shown in Fig. 3.2. These values will be used to construct our statistical model and we refer to them simply as input parameters. Generally, the model closely mirrors NNR input parameters. The evolution of the mean (Fig. 3.2a) and of U1060 is similar in NNR and CM2.1, though the model does show a slightly stronger polar vortex and less variance through January than NNR. In both datasets the mean winds reach a maximum at the beginning of January and become easterly in mid-April. The slight difference in mid-winter can be attributed to the difference in the number of SSWs between model and observations, which would lead to weaker U1060 in January for NNR. The evolution of standard deviation (Fig. 3.2b) is also similar between the climate model and observations. The model slightly underpredicts the standard deviation of U1060. In both datasets, the variability of the polar vortex reaches its maximum in late January (Fig. 3.2b), after the maximum in mean strength (Fig. 3.2a), with a consistent decrease after that. Of note, there is a large seasonal variation in standard deviation so that the maximum in both datasets is more than double that at the beginning of winter.

Our third input into our statistical model is the autocorrelation of U1060 for various days and lags (Fig. 3.2c-e). The different aspects (date and lag) of the correlation are similar between the two datasets, with comparable decorrelation timescales, but minor seasonal differences, most notably in the 10-20 day range. To demonstrate the evolution of correlation over lag, we consider 1 January (Fig. 3.2c) and 15 February (Fig. 3.2d) and their correlations with each other day of winter. Notable for both datasets is the weak anticorrelation at 60 to 75 days lag, possibly indicating oscillatory behavior with a

120-150 day cycle in U1060. NNR is more persistent than CM2.1 through January. This is perhaps related to the persistent nature of SSWs and the increased number of SSWs in NNR. This idea is reinforced by the 15 February autocorrelation. The correlation between this date and all January days is higher in NNR than CM2.1, and it is lower in NNR for days following 15 February, at a time when NNR has fewer SSWs than the model (Fig. 3.2b).

Fig. 3.2e demonstrates the evolution of the lag-1 autocorrelation. This quantity is the only correlation used to calculate the probability of zero crossings. From November to May, the lag-1 autocorrelation tends to increase in both the model and observations. There is a notable exception to this in NNR as February and March have somewhat reduced values, perhaps related to the increased number of SSWs in January. We note that the seasonal evolution of correlations with a higher lag is similar to that of lag-1.

Although not included in our statistical model, the skewness (Fig. 3.2f) provides insight into potential errors caused by our assumption of unskewed normality in the distribution of U1060. A negative skewness implies that the data have more values below the mean than an unskewed normal distribution. More important to our calculations, the negative skewness implies the number of values below zero is larger than in a standard normal distribution. When smoothed, the skewness of the model is more negative than that of the reanalysis. Notably, reanalysis has a positive skewness through March and early April. Some studies have attributed the positive skewness in stratospheric temperature, which implies a negative skewness in stratospheric winds, to the phasing and tilting of upward propagating planetary waves (Watt-Meyer and Kushner 2017).

3.3. Zero Crossings

Zero crossings of U1060 (Fig. 3.3a and b) form the most basic quantity of our statistical model since they are a requirement for all subsequent calculations. In the climate model, empirically determined zero crossings show a low number in early winter (three or fewer for any day in the 10,000 year sample). The increasing strength and relatively low variability of the polar vortex causes this rarity of occurrence. The number of zero crossings maximizes in mid-April, consistent with the time when the mean wind changes from westerlies to easterlies and a near-equal probability of positive or negative U1060. The empirical zero crossings rapidly decrease in May, when the stratospheric winds are very persistent. The empirical zero crossings in NNR show a similar shape, though the trend towards the April maximum is more gradual.

We calculate the probability of a zero crossing by integrating a bivariate normal distribution that implies that U1060 on day $n-1$ is positive and U1060 day n is negative. Our statistical model replicates the above described empirically derived results well. The shape of the distribution is generally correct, with low probabilities in early winter, a gradual increase starting after the polar vortex strength has reached its maximum strength, and a steep decrease in May. Our statistical model also correctly diagnoses that the increase of probabilities in NNR between January and March is not as steep as that in CM2.1. Some minor flaws from our assumptions can be seen early in winter. For both datasets, the statistical approach underpredicts the probability of a zero crossing in the early to mid-winter, while there is a slight overestimate in April. The underestimate is only marginally related to the skewness in the distribution of U1060 during early winter. This is demonstrated by the green curve, which is based on calculations with a bivariate

skew-normal distribution (Azzalini and Dalla Valle 1996), and which only leads to minor improvements. The overestimate at the maximum, though small, could potentially be due to using a lag-1 correlation which is a combination of lower winter values and higher summer values and the nonlinearities which become more important as the correlations approach unity. Our statistical model overestimates the chance of a zero crossing using NNR input data in spring, likely due to sampling uncertainty, but the general shape of the empirically derived evolution is well reproduced.

3.4. Vortex Returns

The probability of vortex returns (Fig. 3.3c and d) is similar to that of zero crossings. Vortex returns are defined as zero crossings with the additional constraint that U1060 becomes positive for 10 consecutive days anytime afterwards. In the empirical data, from November through mid-February, the number of zero crossings and vortex returns is identical. This is because the stratosphere strongly favors westerlies at that time, and 10 consecutive days of westerlies are almost guaranteed to happen. In mid-February, however, the 10 days of westerlies condition will no longer necessarily be fulfilled. Therefore, the probability of vortex returns increases more gradually than that of zero crossings. The vortex return probability reaches a maximum in late February (in both datasets) as the requirement for 10 consecutive days of positive U1060 is increasingly more difficult to fulfill and begins to outweigh the still increasing chance of a zero crossing. There is a steady decrease in vortex return probability through March, and an abrupt drop on 1 April caused by the definition (CP07). The difference in empirically derived vortex returns between the climate model and observations is similar

to that of zero crossings, where observations show more early winter vortex returns than the model. However, the maximum of about 1% per day and its timing in late February is similar in both cases.

To statistically model vortex returns, we use a multivariate normal distribution (Wilks 2006) and sum the likelihood of a vortex return on any day following a zero crossing. We then subtract from it the chance of multiple consecutive 10-day periods of westerlies (see Methods and Appendix). Our statistical model fits well, mirroring the empirical probabilities of zero crossings in early winter, decreasing in slope once the probability of 10 consecutive positive days becomes less than one, and reaching a maximum while the probability of a zero crossing is still increasing. Although our input parameters for CM2.1 and NNR are quite similar (Fig. 3.2), our scheme successfully finds an increase in the probability of a vortex return in January for NNR compared to CM2.1. Thus, subtle differences in the input parameters for our model are important and lead to meaningful differences between the two datasets.

3.5. SSWs

The motivation behind this work aims to model the evolution of SSW probabilities (Fig. 3.4a and b). SSWs differ from vortex returns by simply imposing the restriction that they must occur at least 20 days apart. Empirically (black curves), early in winter, there is very little difference between SSWs and vortex returns. A zero crossing (and therefore vortex return and SSW) is a rare enough event in November and December that the likelihood of two occurring during the same period is miniscule. By late January in the observations, and early February in CM2.1, the 20 days of separation

requirement reduces the slope of the SSW probability curve and causes the maximum in SSWs, while still at the end of February, to decrease to between 0.75% and 0.85% per day. Additionally, in observations, there is a local minimum in the number of SSWs in late January and early February (Fig. 3.2c). This minimum cannot be seen in the number of vortex returns, suggesting the requirement for SSWs to have 20 days of separation is pertinent to why some samples of observations show a maximum of SSWs in January rather than February (Fig. 3.2a).

In our statistical model, we calculate SSW probabilities by multiplying the probability of a vortex return on any given day by the chance that there were no SSWs in the 20 days prior (see methods). The empirically derived annual frequency of SSWs is 0.61 for CM2.1 and 0.64 for NNR. Our statistical model reproduces this well: 0.59 per year for CM2.1 and 0.70 per year for NNR. Using input parameters from either dataset, the maximum daily probability is near 1% and occurs about 10 days later than the empirical maximum. Using NNR, the statistical model produces more SSWs than observed, but the decreasing slope in SSW frequency after mid-January is well reproduced. In both datasets, the underestimate in early winter is balanced by an overestimate in late winter.

3.6. Final Warmings

The overestimate of SSWs and vortex returns and the near-correct estimate of zero crossing in March implies that the statistical model overestimates the chance of positive U1060 in spring after a zero crossing. Thus, if we were to apply our statistical model to final warmings, we would expect it to produce final warmings later than the

empirical data. We define final warmings (Fig. 3.4c and d) as the last zero crossing of U1060 in winter. With our definition, the integral of both the empirical and statistical final warming curves shown in Fig. 3.4c and d are by definition unity, as there is exactly one final zero crossing every winter. In the CM2.1 empirical data, final warmings appear at the beginning of March and maximize in early to mid-April, when the mean of U1060 crosses zero. Observational data show three separate maxima, probably related to large sampling uncertainty. In both datasets, final warmings decrease sharply in May, when the probability of any westerlies in U1060 becomes near zero.

With CM2.1 input parameters, our statistical model produces a curve similar to our empirical data, but as expected, shifted approximately 3 days later. As the lag-1 autocorrelation is slowly increasing in spring (Fig. 3.2e), this provides further evidence that the overestimate of SSWs, as well as underestimate of final warmings in March, is caused by nonlinearities associated with the calculation of correlations. The 3-day shift from the empirical data to the statistical model is maintained through May. If a final warming does not occur earlier in the year, it must occur later, hence the late overestimate. When applied to NNR, our statistical model does produce a somewhat bimodal distribution, which does not occur when modeling zero crossings (Fig. 3.3b).

3.7. Application to Other Models

In order to test whether the success of our statistical model still holds when applied to other datasets, we next use input parameters from a few selected CMIP5 models. The particular models we choose (MIROC5, IPSL-CM5A, and IPSL-CM5B) are outliers in terms of their SSW seasonality (Fig. 3.5). In comparing the input parameters

from these models, we may be able to diagnose to what factors the SSW distribution is most sensitive. The SSW distribution of MIROC5 (Watanbe et al. 2010), a model which we choose because of its lack of SSWs, is well reproduced by our statistical model. The statistical model produces no SSWs throughout the vast majority of winter, with a very small chance in late March. Also of note, zero crossings are narrowly clustered around mid-April, which is again well represented by our statistical model. From a brief analysis of our input parameters, the mean and correlations of CM2.1 are similar to that of NNR and CM2.1, but the standard deviation in MIROC5 is much too small. Thus, the lack of variability in polar vortex strength can be directly related to the lack of SSWs. The opposite is true in IPSL's CM5A (Dufresne et al. 2013), which we choose because of its large number of SSWs compared to most other CMIP5 models. Our statistical model again represents the empirical number of SSWs and zero crossings well, except that the decrease in SSWs in late March is less pronounced. From the input parameters, it is clear that this is related to the increased standard deviation in U1060, as the means and correlations are similar to CM2.1 (Fig. 3.2). Finally, we examine IPSL's CM5B (Dufresne et al. 2013), which has a January SSW maximum as opposed to the usual February maximum in most other models. Again, our zero crossing calculations fit well, though we still have somewhat an underestimate of both zero crossings and SSWs in January. Even though the mean U1060 of CM5B is higher than in any other dataset, the January maximum may be explained by the maximum in standard deviation during that month. Sampling variability also plays a role as this dataset contains only 95 years of data. Through the comparison of these three models, the standard deviation of U1060 appears to be a strong predictor for the occurrence of SSWs.

3.8. Sensitivity Analysis

The skewness in U1060 in early winter (Fig. 3.2f) indicates a limitation of our assumption of an unskewed normal distribution. This assumption results in a reduced number of U1060 values below zero compared to the negatively skewed empirical distribution. Although the numerical algorithm we use to calculate the integral of a multivariate normal distribution (Genz et al. 2004) does not incorporate skewness, we attempt to account for this underestimate by simply shifting the mean of our daily unskewed normal distributions toward smaller U1060. By doing so, we accurately represent the percent of values of U1060 below zero for any given day in our empirical dataset. We then use the same correlation and standard deviation as before for our input parameters to refine our calculation of SSW probability. The new calculations (Fig. 3.6a) yield results that align very well with the distribution of SSWs in CM2.1 until late February, when we again see the overestimate. This suggests that the neglect of skewness is the leading cause for the issues in early winter. In late winter and spring, however, the remaining overestimate provides more evidence that the errors are caused largely by different autocorrelations between summer and winter and our input parameters being calculated from a combination of the two. When applied to NNR (Fig. 3.6b), there is a consistent overestimate of SSWs. This may potentially be explained in late winter by the positive skewness in NNR (see Fig. 3.2 a) around the spring equinox, overestimating the number of vortex returns after a zero crossing.

Going back to our CM2.1 climate model and realizing the importance of the standard deviation of U1060 leads us to ask how sensitive our model is to the seasonal changes in both standard deviation and correlation. We know that zero crossings and

SSWs are sensitive to the evolution of mean U1060 because a zero crossing is more likely when the mean is increasing over time than when it is decreasing. This (along with a higher mean and lower standard deviation) explains why November and December have far fewer SSWs and zero crossings than February and March. Therefore, we rerun our statistical model many times for CM2.1 using constant standard deviations ranging from 4 m/s to 20 m/s (Fig. 3.7a). Unsurprisingly, there is a considerable change in the shape of the distribution consistent with standard deviation being the denominator of our limits of integration (Eq. 1). In all cases the minimum probability of SSWs is at the maximum of mean U1060, which goes to near zero when the constant is at its lowest values. As a reference, mean of U1060 on 1 November is approximately equal to that on 25 February (Fig. 3.2a). The lowest constant standard deviation (4 m/s) results in a statistical output in which SSWs exclusively occur in March, similar to what we what we found for MIROC5 (Fig 3.6). When the standard deviation increases to 8 m/s, the number of SSWs in November is already higher than in the original model. As the standard deviation increases, as expected, the SSW probability increases on all days, and the late winter maximum becomes earlier. At the highest standard deviation (20 m/s), the maximum probability of an SSW is on 1 November. This is an artificial product of calculating if the polar vortex returns through only 31 May (see Methodology); a large prescribed standard deviation of U1060 applied to all days removes the guarantee of a final warming.

We next explore the impact of variations in the autocorrelation of U1060. To this end, we modify our original correlation matrix, $r(t, \tau)$, to become the same for all dates t and therefore become simply $r(\tau)$, a function of lag only. We begin by using the mean

over all days of the year for each lag (blue curve, Fig. 3.7b). Doing so has very little impact on the outcome. We then approximate $r(\tau)$ by an exponential function using a least squared fit to the mean lagged correlations found previously. Because we suspect that correlations at short lags dominate our statistical model, we rerun the model many times using exponential fits starting at lag-0 and incorporating an increasing number of lags (lag-1, lag-2, lag-10, red curves, Fig. 3.7b). The lag-10 fit underestimates autocorrelation at short lags, leading our statistical model to overestimate the probability of an SSW. Lag-1 leads to the opposite. Using lag-2 most closely resembles our original statistical model, confirming our original assumption that our model is most sensitive to autocorrelation at short lags. Notably, the shapes of all three correlation-modified models are similar and maximize on the same day as our original model. Therefore, we conclude that autocorrelation does not impact the seasonal SSW distribution; however, it does impact the magnitude of the maximum probability and in turn the annual number of SSWs.

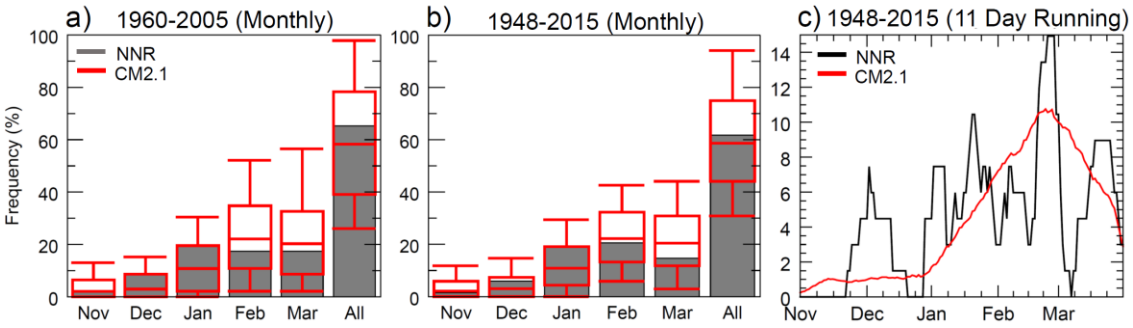

Fig 3.1. SSW climatology for CM2.1 and NNR. Shown are (red) the monthly mean, minimum, maximum, and 95% confidence interval of SSW frequency in the CM2.1 model derived from bootstrapping (left) 45 winters and (center) 67 winters 10,000 times. Gray bars are the corresponding frequency of SSWs in NNR. C) shows the frequency of SSWs within an 11-day sliding interval in (black, 67 years) NNR and (red, 10,000 years) CM2.1 data.

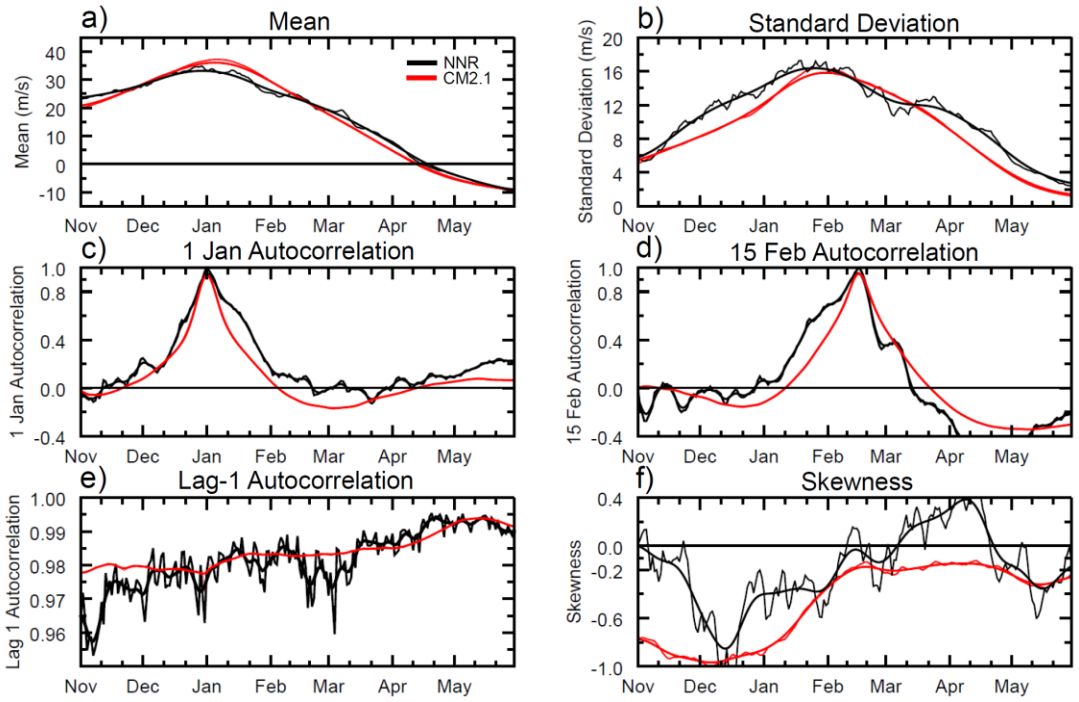

Fig. 3.2. Input parameters of U1060 for the statistical model. C) and D) show the correlation for 2 base days with any other day in winter. E) shows the lag-1 correlation for all base days in winter.

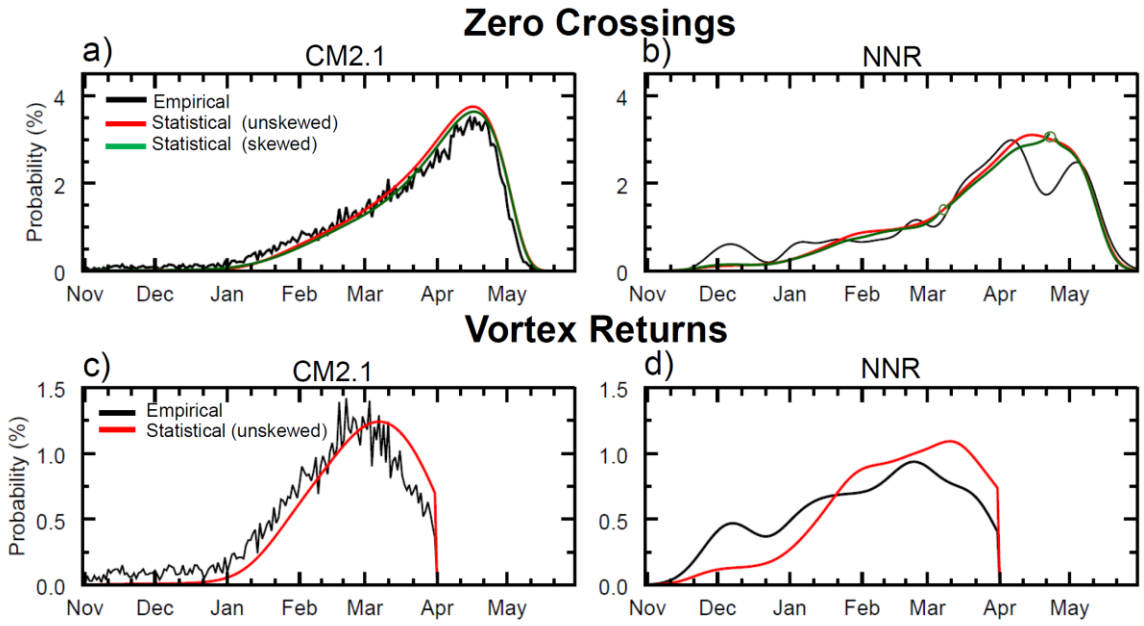

Fig 3.3. Zero crossings and vortex returns (probabilities in % per day). Zero crossings show (black) empirical data, and output from the statistical model using a (green) bivariate skew-normal and (red) unskewed bivariate normal distribution of U1060. Vortex returns show (black) empirical results and output from the statistical model with a (red) unskewed normal distribution.

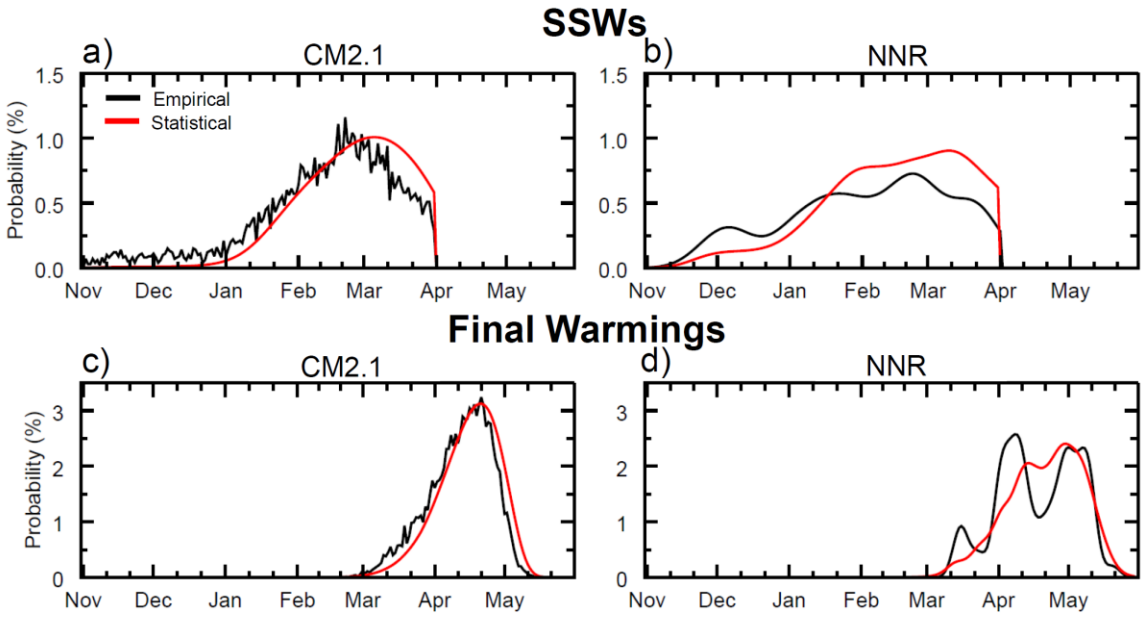

Fig. 3.4. SSWs and final warmings. See Fig. 3.3 for details.

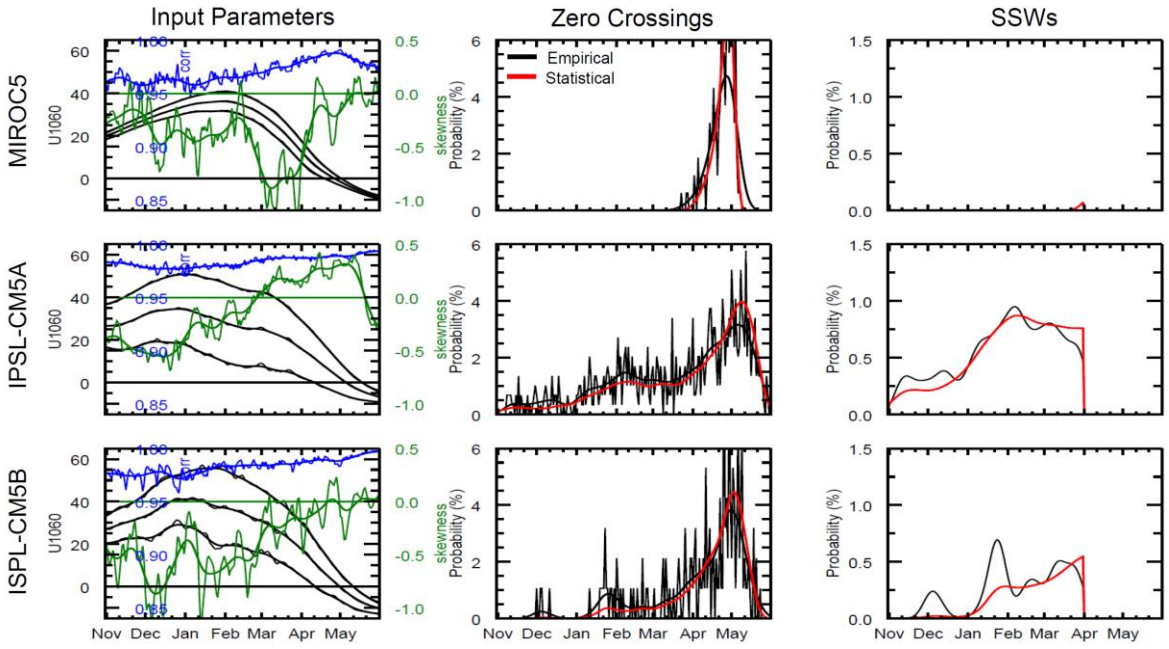

Fig. 3.5. Results from additional models. The models are MIROC5 (historical run 2, 1850-2012), IPSL's CM5A (medium resolution, RCP45, 2006-2300), and IPSL's CM5B (low resolution, RCP85, 2006-2100). Input parameters show (black) the mean of U1060 plus or minus one standard deviation, (blue) the lag-1 correlation, and (green) the skewness. Empirical values and a smoothed version of it are shown in each case. For zero crossings and SSWs, black are the empirical data (smoothed) and red the statistical model output.

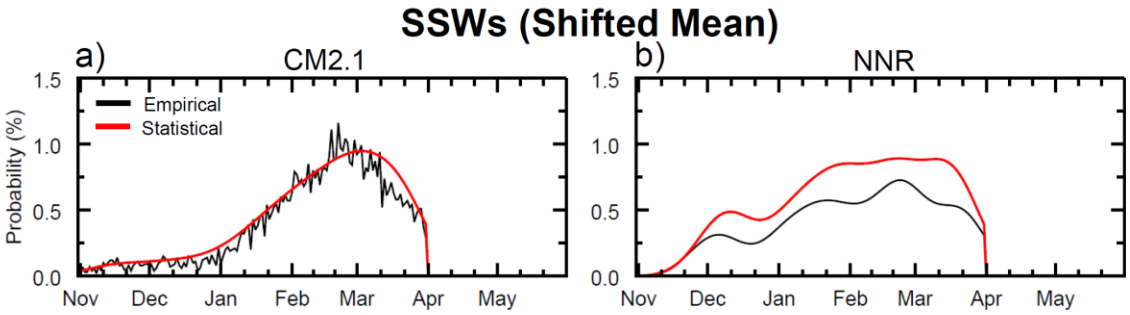

Fig. 3.6. SSWs for adjusted input. Shown are SSW calculations with the mean of U1060 each day adjusted to account for the skewness in U1060 (see text for details). For NNR, both (red) statistical and (black) empirical data have been smoothed.

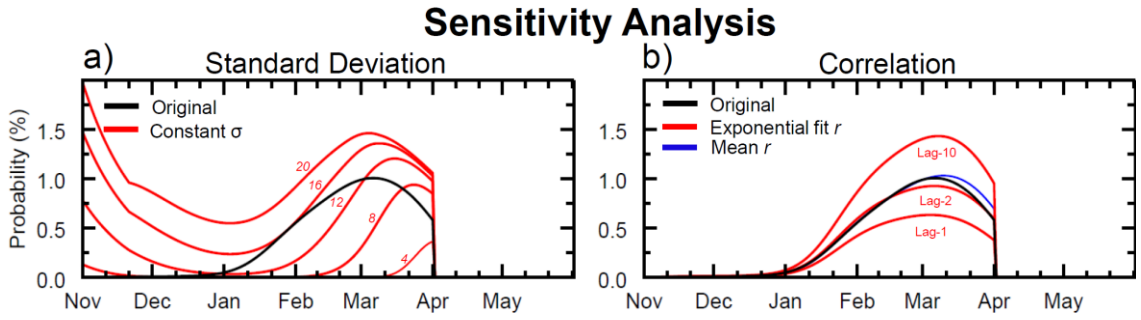

Fig. 3.7. Sensitivity analysis. Shown are (black) the original results from our statistical model and (left, red) the result when standard deviation (in m/s) is set to a constant throughout the year. (Right) shows results from using constant lagged correlations when (blue) all lagged correlations are set to their mean using all days of the year, and (red) correlation is approximated by a least square fit considering only days 0-1 (lag-1), days 0-2 (lag-2), and days 0-10 (lag-10).

CHAPTER 4

CONCLUSION

The motivation for this work stems from the large sampling uncertainty when determining the seasonal cycle of SSWs. The monthly distribution is used as a metric of performance for GCMs, and we attempt to determine if GCMs with a late winter maximum of SSWs are truly inconsistent with observations. It is further influenced by the interplay between polar vortex strength and stratospheric wave driving, and how the evolution of both impacts this seasonal cycle. We aim to find which is more important in controlling the seasonal distribution of SSWs. To investigate these questions, we create a simple statistical model that uses only the daily climatology of U1060 as the input and assumes stratospheric winds follow a multivariate normal distribution. Using this statistical model, our goal is to recreate the seasonal distribution of the 4 events described in the methodology seen in both reanalysis and the climate model.

Overall, the results of the statistical model (Fig. 4.1) reflect what is seen the climate model. The statistical output is generally correct in magnitude; the daily probability of all events increases at the same time as the statistical model, and the transition from winter westerlies to summer easterlies is well reproduced. Although there are a few minor discrepancies between the statistical model and the empirical data, which are discussed in the results, most of these differences are seen in the zero crossings which

do not fit our criteria for either SSWs or final warmings. If SSWs are extremely rare events, our initial assumption of normality should prove to be inaccurate. However, the success of our statistical model, which ignores the skewness of the distribution, indicates that stratospheric winds can be approximated by a normal distribution in U1060 and that SSWs simply form the tail of this distribution. Coughlin and Gray (2009) hypothesize that there is a well-separated warm state and cold state in the stratosphere, and that all SSWs are members of the warm state. The results found by our model imply that all values of zonal mean zonal wind can be instead described with one continuous distribution.

The success of the statistical model indicates that the frequency of empirical SSWs closely follows the number of SSWs implied by the evolution of U1060. Planetary wave propagation is taken into account in this model only by its impact on the mean and standard deviation of U1060. Because the statistical model indicates that the most SSWs occur long after the maximum in planetary wave propagation, we assess that the primary factor in the temporal distribution of SSWs is the climatological strength of the polar vortex. The mid-winter increase in planetary wave propagation has secondary effects, but the stronger vortex in mid-winter is a larger suppressor of SSWs than the maximum in EP flux is an aid. We cannot completely discount the need for increased stratospheric wave driving, as the statistical model is very sensitive to the value of standard deviation. However, this study provides further evidence that there is a sufficient amount of stratospheric wave driving in the Northern Hemisphere to cause SSWs at any point during the winter.

Returning to our initial goal and motivation, we find that the mid-winter

maximum of SSWs can very likely be attributed to sampling uncertainty. Using bootstrapping, we cannot reject with 95% confidence the null hypothesis that the monthly distribution in CM2.1 and NNR come from the same population. Additionally, when adjusting our bin size to a smaller interval, the observational maximum occurs at the same time as our model maximum. Considering our previous assessment that a weakening polar vortex is more important to the occurrence rate of SSWs than the amount of stratospheric wave driving, we expect that future SSWs will occur more often in late winter than mid-winter, causing a shift in the overall distribution of SSWs in observations.

It should be noted that all input parameters to our statistical model take into account SSWs that occurred. This study does not differentiate between years with SSWs and without SSWs, and does not consider the direct causes for or impacts of SSWs. It does provide evidence of when during the winter season to expect the greatest likelihood for an SSW and what conditions favor SSWs. It also provides ideas for evaluating stratospheric dynamics of GCMs while taking into account the small sample size of observed SSWs.

Our results lead to several questions to investigate in future work. The daily mean of U1060 and the amount of upward propagating waves evolve in similar manners through the winter (Fig 1.1). It may be possible to develop a similar model using the evolution of EP-Flux, or to develop an index using both factors that is more accurate than this model. Our statistical model systematically underestimates the number of early winter SSWs, but is more accurate while the strength of the polar vortex is decreasing. This is partially due to not taking into account the skewness of the distribution, but future

work can determine how the stratosphere acts while the polar vortex is strengthening to determine if there are separate dynamics behind, or more importantly, effects of, early and late winter SSWs. Early winter SSWs may be mostly a product of planetary wave propagation while late winter SSWs are primarily a product of the decreasing strength of the polar vortex. As either computing speed or mathematics progress, it may also be possible to directly incorporate the original skewness of the distribution into the model. Lastly, in future analysis of the stratospheric dynamics of GCMs, it would be prudent to not consider a late winter maximum in SSWs as an indicator of flaws in those models' portrayal of the stratosphere. The evolution of stratospheric winds at any latitude and level consistent with the polar vortex would be a much more appropriate performance metric.

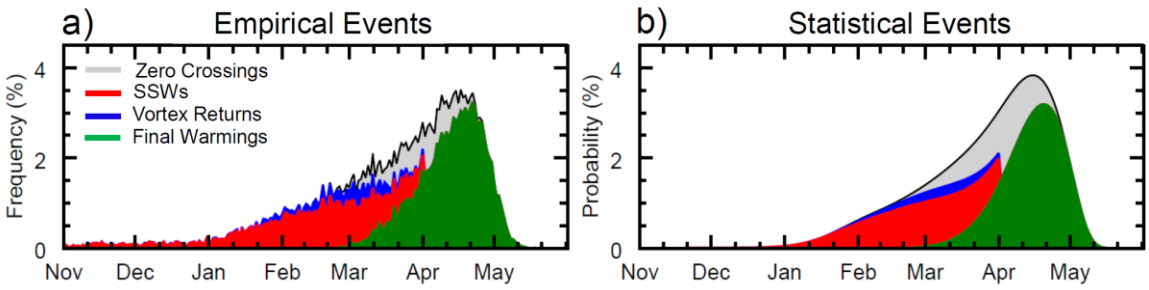

Fig 4.1. Overview of statistical results for CM2.1. Shown are (red) SSWs, (blue) vortex returns, (green) final warmings, and (grey) zero crossings from (left) empirical CM2.1 data and (right) our statistical model using CM2.1 inputs. Red areas are a subset of blue areas. Blue and Green areas are mutually exclusive subsets of the grey area.

APPENDIX

VORTEX RETURN CALCULATIONS

Our vortex return calculations are created with a series of nested integrals. For all purposes, the equation integrated the multivariate normal distribution (Eq. 1), however the number of integrals we take alters based off when the time of 10 days of positive U1060 starts. In the following, to represent any days of positive U1060, the lower limit of integration is $-\frac{\mu_k}{\sigma_k}$ where k is the day of interest, while the upper limit of integration is ∞. To represent days of negative U1060, the lower limit of integration is $-\infty$ while the upper limit of integration is $-\frac{\mu_k}{\sigma_k}$.

A vortex return on day *n* requires 10 consecutive days of positive U1060 on any day after a zero crossing. We sum the chance of U1060 becoming positive starting the day after the zero crossing until 22 May, which is the last day where 10 consecutive days of U1060 could be positive ending 31 May. However, the calculation changes depending on how many days after the initial zero crossing (hereafter day *n*) it takes for this period of 10 consecutive days of positive U1060 to begin. To represent the zero crossing returning on day *n+1*, we use a 12-dimensional integral where day *n-1* has positive U1060, day *n* has negative U1060, and days *n+1* through *n+10* have positive U1060. For the 10 consecutive days of positive values starting on day *n+2* though *n+11*, we must also consider that the day before these 10 days of positive U1060 has a negative U1060.

Therefore, we use a 13-dimensional integral representing day *n-1* with positive U1060, day *n* and the day prior to the 10 consecutive days with a negative U1060, and the 10 consecutive days again with a positive U1060.

Beginning with day *n+12*, we must consider the probability that there have already been 10 consecutive days of positive U1060. For these days, we begin with the same 13-dimensional integral described to determine if these start on day *n+2* though *n+11*. We then subtract the value of a 22-dimensional integral, which calculates the probability day *n-1* had a positive value of U1060, day *n* had a negative value of U1060, day *n+1* through *n+10* had a negative U1060 the day before these 10 consecutive days had a negative U1060 and the 10 days of interest again showed a positive value. Starting day *n+13* (the 23-dimensional integrals are unnecessary on day *n*+12) through 22 May, we also subtract as many 23-dimensional integrals as necessary which imply that the first 10 consecutive days of positive U1060 happened after day *n+1* but before the day of interest.

REFERENCES

Albers, J. and T. Birner, 2014: Vortex Preconditioning Due to Planetary and Gravity Waves Prior to Sudden Stratospheric Warmings. *J. Atmos. Sci.,* **71**, 4028–4054, doi: 10.1175/JAS-D-14-0026.1.

Azzalini, A. 1985: A Class of Distributions which Include the Normal Ones. *Scand. J. Stat.*, **12**, 171-178, stable URL: http://www.jstor.org/stable/4615982.

Azzalini, A. and A. Dalla Valle, 1996: The Multivariate Skew-Normal Distribution. *Biometrika*, **83**, 715-726, doi: 10.1093/biomet/83.4.715.

Baldwin, M., and T. Dunkerton, 2001: Stratospheric Harbingers of Anomalous Weather Regimes. *Science*, **294**, 581–584. doi: 10.1126/science.1063315

Baldwin, M, D. Stephenson, D. Thompson, T. Dunkerton, A. Charlton, and A. O'Neill, 2003: Stratospheric Memory and Skill of Extended-Range Weather Forecasts. *Science*, **301**, 636–640, doi: 10.1126/science.1087143.

Black, R., B. McDaniel, and W. Robinson, 2006: Stratosphere–Troposphere Coupling During Spring Onset. *J. Climate*, **19**, 4891–4901, doi: 10.1175/JCLI3907.1.

Butchart, N. and Coauthors 2011: Multimodel Climate and the Variability of the Stratosphere. *J. Geophys. Res.: Atmos.*, **116**, D05102, doi: 10.1029/2010JD014995.

Butler, A., D. Seidel, S. Hardiman, N. Butchart, T. Birner, and A. Match, 2015: Defining Sudden Stratospheric Warmings. *Bull. Amer. Meteor. Soc.*, **96**, 1913–1928, doi: 10.1175/BAMS-D-13-00173.1.

Charlton, A., A. O'Neill, W. Lahoz, A. Massacand, and P. Berrisford, 2005: The Impact of the Stratosphere on the Troposphere During the Southern Hemisphere Stratospheric Sudden Warming, September 2002. *Q. J. R. Meteorol. Soc.,* **131**, 2171-2188, doi: 10.1256/qj.04.43

Charlton, A and L. Polvani, 2007: A New Look at Stratospheric Sudden Warmings. Part I: Climatology and Modeling Benchmarks. *J. Climate*, **20**, 449–469, doi: 10.1175/JCLI3996.1.

Charlton, A and Coauthors, 2007: A New Look at Stratospheric Sudden Warmings. Part II: Evaluation of Numerical Model Simulations. *J. Climate,* **20,** 470-488, doi:

10.1175/JCLI3994.1.

Charlton-Perez, A., L. Polvani, J. Austin, and F. Li, 2008: The Frequency and Dynamics of Stratospheric Sudden Warmings in the 21st century. *J. Geophys. Res.*, **113**, D16116, doi:10.1029/2007JD009571.

Charlton-Perez, A. and Coauthors, 2013: On the Lack of Stratospheric Dynamical Variability in Low-Top Version of the CMIP5 Models. *J. Geophys. Res.*, **118**, 2494-2505, doi: 10.1002/jgrd.50125

Coughlin, K. and L. Gray, 2009: A Continuum of Sudden Stratospheric Warmings. *J. Atmos. Sci.*, **66**, 531–540, doi: 10.1175/2008JAS2792.1.

Delworth, T. and Coauthors, 2006: GFDL's CM2 Global Coupled Climate Models. Part I: Formulation and Simulation Characteristics. *J. Climate*, **19**, 643–674, doi: 10.1175/JCLI3629.1.

Dufresne, J. and Coauthors, 2013: Climate Change Projections Using the IPSL-CM5 Earth System Model: from CMIP3 to CMIP5, *Climate Dyn.*, **40**, 2123, doi:10.1007/s00382-012-1636-1

Genz, A., F. Bretz and Y. Hochperg, 2004: Approximation to Multivariate t Integrals with Application to Multiple Comparison Procedures, *Recent Developments in Multiple Comparison Procedures, Institute of Mathematical Statistics LNMS*, **47**, 24-32. (code retrieved 2 December 2016 from http://www.math.wsu.edu/faculty/genz/homepage)

Holton, J. and G. Hakim, 2013: *An Introduction to Dynamic Meteorology, Fifth Edition*, Academic Press, 532 pp.

Ineson, S. and A. Scaife, 2009: The Role of the Stratosphere in European Climate Response to El Nino, *Nat. Geosci.*, **2**, 32-36, doi:10.1038/ngeo381.

Jucker, M., 2016: Are Sudden Stratospheric Warmings Generic? Insights from an Idealized GCM., *J. Atmos. Sci.*, **73,** 5061-5080, doi: 10.1175/JAS-D-15-0353.1.

Kalnay, E. and Coauthors, 1996: The NCEP/NCAR 40-Year Reanalysis Project, *Bull. Amer. Meteor. Soc.*, **77**, 437-471, doi: 10.1175/1520-0477(1996)077<0437:TNYRP>2.0.CO;2.

Kidston, J., A. Scaife, S. Hardiman, D. Mitchell, N. Butchart, M. Baldwin and L. Gray, 2015: Stratospheric Influence on Tropospheric Jet Streams, Storm Tracks and Surface Weather. *Nat.Geosci.*, **8**, 433-440, doi: 10.1038/ngeo2424

Krüger, K., B. Naujokat, and K. Labitzke, 2005: The Unusual Midwinter Warming in the Southern Hemisphere Stratosphere 2002: A Comparison to Northern Hemisphere

Phenomena. *J. Atmos. Sci.*, **62**, 603–613, doi: 10.1175/JAS-3316.1.

Matsuno, T., 1971: A Dynamical Model of the Stratospheric Sudden Warming. *J. Atmos. Sci.*, **28**, 1479–1494, doi: 10.1175/1520-0469(1971)028<1479:ADMOTS>2.0.CO;2

Polvani. L and D. Waugh, 2004: Upward Wave Activity Flux as a Precursor to Extreme Stratospheric Events and Subsequent Anomalous Surface Weather Regime. *J. Climate*, **17**, 3548-3554, doi: 10.1175/1520-0442(2004)017<3548:UWAFAA>2.0.CO;2.

Sigmond, M., J. Scinocca, V. Kharin, and T. Shepherd, 2013: Enhanced Seasonal Forecast Skill Following Stratospheric Sudden Warmings. *Nat. Geosci.*, **6**, 98–102, doi:10.1038/ngeo1698.

Staten, P. and T. Reichler, 2013: On the Ratio Between Shifts in the Eddy-Driven Jet and the Hadley Cell Edge, *Climate Dyn.,* **42**, 1229-1242, doi:10.1007/s00382-013-1905-7.

Thompson, D., M. Baldwin, and J. Wallace, 2002: Stratospheric Connection to Northern Hemisphere Wintertime Weather: Implications for Prediction. *J. Climate,* **15**, 1421–1428, doi: 10.1175/1520-0442(2002)015<1421:SCTNHW>2.0.CO;2.

Watanbe, M. and Coauthors, 2010: Improved Climate Simulation by MIROC5: Mean States, Variability, and Climate Sensitivity. *J. Climate*, **23**, 6312-6335, doi: 10.1175/2010JCLI3679.1.

Watt-Meyer, O. and P. Kushner, 2017: Why are Temperature and Upward Wave Activity Flux Positively Skewed in the Polar Stratosphere? *Unpublished Manuscript.*

Wilks, D. 2006: *Statistical Methods in the Atmospheric Sciences, Second Edition*, Academic Press, 627 pp.